

# Incorporating multiple grid-based data in CNN-LSTM hybrid model for daily runoff prediction in the source region of the Yellow River Basin

Feichi Hu<sup>a</sup>, Qinli Yang<sup>a,\*</sup>, Junran Yang<sup>a</sup>, Zhengming Luo<sup>a</sup>, Junming Shao<sup>b</sup>, Guoqing Wang<sup>c</sup>

<sup>a</sup> School of Resources and Environment, University of Electronic Science and Technology of China, No. 2006, Xiyuan Avenue, Chengdu 611731, China

<sup>b</sup> School of Computer Science and Engineering, University of Electronic Science and Technology of China, No. 2006, Xiyuan Avenue, Chengdu 611731, China

<sup>c</sup> State Key Laboratory of Hydrology-Water Resources and Hydraulic Engineering, Nanjing Hydraulic Research Institute, Nanjing 210029, China



## ARTICLE INFO

### Keywords:

Deep learning  
Dynamic representation  
Runoff prediction  
Ungauged regions  
Source region of the Yellow River basin

## ABSTRACT

*Study region:* The Source Region of the Yellow River Basin (SRYRB), China

*Study focus:* To improve daily runoff prediction accuracy in data-scarce areas, this study focuses on incorporating multiple grid-based data (precipitation, EVI, soil moisture (SM)) to drive the CNN-LSTM hybrid model. The spatial features of precipitation and underlying surface of the basin can be extracted by CNN, while the temporal features of the input data series can be captured by the LSTM. The hybrid model is compared with the single models (CNN, LSTM), and hybrid model performances under different driven data are also investigated.

*New hydrological insights for the region:* Driven by the in-situ precipitation, grid-based precipitation (GPM) and SM data, the CNN-LSTM hybrid model achieved the best prediction result with NSE of 0.834, outperforming the single LSTM model ( $\text{NSE}=0.510$ ) and the CNN model ( $\text{NSE}=0.612$ ). It indicates that the hybrid model captures the spatiotemporal change features of precipitation and underlying surface of the basin. When using only GPM and SM data as input, the hybrid model achieved comparable result with NSE of 0.827. It implies that GPM could serve as a good alternative of in-situ precipitation and SM could provide additional value to improve prediction. This study highlights the value of using multiple grid-based data to drive the hybrid model, which provides new insights into runoff prediction in data-scarce regions.

## 1. Introduction

Runoff prediction plays important roles in the scientific study of hydrological evolution mechanisms as well as various practical applications such as flood and drought defense (Ibrahim et al., 2022; Xu et al., 2022). As the member of complex hydrological dynamic evolution system, the runoff generation and variation are simultaneously affected by climate factors, underlying surfaces, and human activities (Jin et al., 2021; Zhou et al., 2021). Therefore, in such a complex circumstance, where different impact factors interact and feedback with each other, accurate runoff prediction remains challenging up to the present.

\* Corresponding author.

E-mail address: [qinli.yang@uestc.edu.cn](mailto:qinli.yang@uestc.edu.cn) (Q. Yang).

Various hydrological models have been developed for runoff prediction, primarily categorized into process-based models and data-driven models. Process-based models can be further divided into distributed or semi-distributed models (such as MIKE SHE (Ma et al., 2016), Soil and Water Assessment Tool (SWAT) (Gassman et al., 2014)) and lumped models (such as Tank (Lee and Singh, 2005), XAJ (Shi et al., 2011)). Data-driven models encompass methods like Autoregressive Moving Average (ARMA) (Abrahart and See, 2000), Support Vector Regression (SVR) (Dibike et al., 2001), Random Forest (RF) (Breiman, 2001), XGBoost (Chen and Guestrin, 2016), data stream model (Yang et al., 2019), and Artificial Neural Networks (ANNs) (Tokar and Johnson, 1999), among others. These models rise in different basin contexts and demonstrate excellent performance. Among them, ANNs have become one of the most popular methods worldwide in recent years (Lv et al., 2020). ANNs possess excellent learning capabilities, strong ability to handle non-linear relationships, and are relatively easy to understand and implement (Mishra et al., 2016; Sit et al., 2020; T. Xu and Liang, 2021). Riad et al. (2004) demonstrated that ANNs outperform classical regression models in runoff prediction.

As a member of the ANNs, Long Short-Term Memory (LSTM) stands out in the field of hydrology due to its advanced time series learning capabilities and the ability to solve the gradient disappearance or gradient explosion problems of ordinary recurrent neural networks (Staudemeyer and Morris, 2019; Li et al., 2021; Yin et al., 2021). Yuan et al. (2018) calibrated the parameters of LSTM using ant-lion optimizer and achieved high-precision prediction of monthly-scale runoff. Xiang et al. (2020) applied a fusion model of LSTM and seq2seq for rainfall-runoff prediction at hourly scale in Iowa, improving the accuracy of short-term flood forecasting. Man et al. (2023) increased the predictive capacity of LSTM for peak runoff by adding a loss function. These cases demonstrate the excellent performance of LSTM in the field of runoff prediction.

However, due to the structural design of LSTM, most existing LSTM based models for runoff prediction can only take gauge-based meteorological sequences data (1-dimensional) instead of grid-based data (2-dimensional) as input. With the development of deep learning, the CNN-LSTM hybrid model has been proposed, which combines the strength of CNN in spatial feature extraction from 2-dimensional data and the strength of LSTM in temporal feature learning (Luan and Lin, 2019; Yan et al., 2021). However, most applications of CNN-LSTM model in runoff prediction either use 1-dimensional data as input or only take one type of 2-dimensional data into account. For instance, Zhou et al. (2023) proposed an SA-CNN-LSTM model that uses only rainfall and runoff sequences as input for runoff prediction. Li et al. (2022) used a CNN-LSTM model to process 2-dimensional rainfall radar data and upstream runoff sequences for runoff prediction. Actually, grid-based data such as GPM, EVI and SM represent spatial heterogeneity of meteorology and underlying surface of a basin which play important roles in runoff prediction (Shen et al., 2017; Xin et al., 2021).

SRYRB is a crucial water conservation area for the Yellow River, accounting for 34.5% of the annual runoff (Meng et al., 2016). Runoff prediction in this region is highly beneficial. However, due to complex and variable terrain, with an average elevation of around 4000 m, the basin is sparsely gauged with limited hydro-meteorological station, belonging to data scarce region (Li et al., 2016; Liu et al., 2023). To address the issue, Yang et al. (2023) proposed a monthly runoff prediction model based on few-shot learning; Guan et al. (2019) improved the GR4J model achieving a Nash-Sutcliffe Efficiency (NSE) of 0.832 within the basin. However, runoff prediction in the data-scarce region (SRYRB) is still challenging.

Besides the in-situ data, remote sensing data and reanalysis data can provide valuable data characterizing meteorology and underlying surface of basins (Moukomla and Blanken, 2017; Zhou et al., 2017). Some studies have demonstrated the value of remote sensing data in hydrological modeling. Kwon et al. (2020) proposed a rainfall-runoff model that combines conceptual hydrological models, SVM, and remote sensing-based soil moisture data, which outperformed traditional Tank model in low-flow simulations. Islam et al. (2023) used remote sensing data for Random Forest Machine Learning Analysis (RFML) in streamflow prediction, showing higher accuracy than SWAT. Reanalysis data, on the other hand, are derived from physical models, can also offer long-term, spatially seamless, and consistent data, which are valuable for long-term trend analysis (Bengtsson et al., 2004; Balsamo et al., 2015).

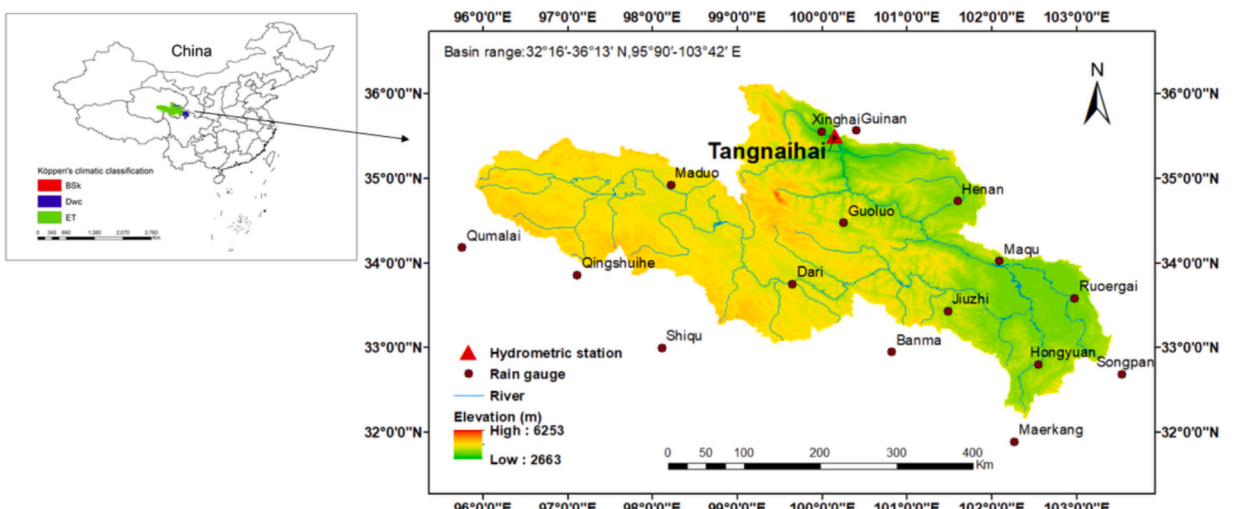


**Fig. 1.** The research area and the distribution of rain gauges and hydrometric station.

Therefore, to improve runoff prediction accuracy in the SRYRB, this study aims to incorporate multiple grid-based data into the CNN-LSTM hybrid model. The objectives of this study are as follows: (1) Incorporate remote sensing based GPM and EVI data, reanalysis based soil moisture data into the CNN-LSTM hybrid model. (2) Validate the performances of the CNN-LSTM model under different driven data sources in the SRYRB. (3) Explore the feasibility of the proposed model in un-gauged basin.

## 2. Study area and data acquisition

### 2.1. Study area

This study selected the Source Region of the Yellow River Basin (SRYRB) (Fig. 1) as a case study. The basin usually refers to the upstream area of the Yellow River above the Tangnaihai hydrometric station. Its area accounts for 15.4% of the total area of the Yellow River Basin (Yuan et al., 2015), and its runoff accounts for 34.5% of the annual runoff of the Yellow River (Meng et al., 2016). Restricted by high altitude (ranging from 2663 to 6253 m) and complex geographical conditions, the study area is sparsely gauged with only 9 gauges established in the basin, resulting in a relative lack of hydrological data in the region. This data scarcity creates challenges for hydrological model building and validation, while also providing an opportunity to research and improve hydrological prediction methods.

The basin has a typical plateau continental climate and is in the transitional zone between the plateau subarctic and plateau temperate zones. The Köppen climate classification of the basin is mainly ET (Polar, tundra) and Dwc (Cold, dry winter, cold summer). Among them, the southeastern part of the basin and the lower reaches of the river are dominated by Dwc, and the remaining areas are dominated by ET. Its main climate is characterized by alternating cold and hot periods, distinct dry and wet seasons, small annual temperature differences, large daily temperature differences, no clear four-season distinction, and strong sunshine. The annual average temperature in the basin ranges from  $-4$  to  $-5$  °C (Song et al., 2009), and the average annual precipitation is between 220 and 780 mm (Ren et al., 2022), both increasing from west to east and from north to south as altitude decreases. Precipitation is unevenly distributed throughout the year, with the flood season (June to September) accounting for approximately 60% of the annual rainfall. The SRYRB has complex landforms including high mountains, basins, gorges, plateaus, and numerous lakes (Guo et al., 2022). Alpine vegetation is the main vegetation type, with alpine meadows and alpine grasslands accounting for about 80% of the total area.

### 2.2. Data acquisition

The data used in this study include three types: gauge-based (in-situ) data, remote sensing data and re-analysis data. Gauge-based data include daily precipitation data at 16 rain gauges and daily runoff data from 1 hydrometric station. Three types of 2D data are selected: precipitation, enhanced vegetation index (EVI) and soil moisture to effectively represent meteorological factors and underlying surface characteristics. Specifically, remote sensing data comprise precipitation (GPM\_3IMERGDF) and EVI (MOD13A1). Reanalysis data comprise soil moisture (ERA5-Land). The reasons for these choices are detailed in following paragraphs. Table 1 summarizes the basic information of these datasets. To keep consistency and continuity of the time series of all variables, the study finally chooses 2007–2014 as the study period.

The Global Precipitation Measurement (GPM) is an international satellite mission jointly conducted by the National Aeronautics and Space Administration (NASA) and the Japan Aerospace Exploration Agency (JAXA) (Smith et al., 2007). It utilizes multiple sensors, satellites, and algorithms to derive more accurate precipitation data. It provides global, microwave-based precipitation data products within 3 h and infrared-microwave- based precipitation and snowfall data products within half an hour (Pradhan et al., 2022). GPM IMERG is one of the most accurate precipitation data available (Tang et al., 2020). The earliest data available is from 2000. This study uses the GPM IMERG Final Precipitation L3 1 day 0.1-degree x 0.1-degree (GPM\_3IMERGDF) data, which represents the final estimate of the daily accumulated precipitation.

The enhanced vegetation index (EVI) is an index used for remote sensing satellite image analysis and vegetation monitoring, and is more applicable to a wide range of vegetation types. The EVI data are from the MOD13A1 - MODIS/Terra Vegetation Indices 16-Day L3 Global 500 m SIN Grid provided by NASA/USGS. The dataset can minimize the changes in the crown background and maintain sensitivity to dense vegetation conditions; while using the blue band to eliminate residual atmospheric pollution caused by smoke and sub-pixel thin clouds. The earliest data available in this dataset is from 2000.

ERA5-Land is a reanalysis dataset that provides high-resolution, multi-decadal land variable evolution. Its reanalysis method combines model data with observation results worldwide using physical laws to form a global and consistent dataset. Compared with

**Table 1**

Summary of the data sets used in this study.

Data source	Variable	Resolution	Frequency	Coverage	Period	Producer
GPM_3IMERGDF	Precipitation	10 km	1d	Global	2000-present	GES DISC
MOD13A1	EVI	500 m	15d	Global	2000-present	NASA/USGS
ERA5-Land	Soil moisture	0.1°	1 h	Global	1950-present	ECMWF
Rain gauges	Precipitation	/	1d	16 sites	1960-2018	CMA
Hydrometric station	Runoff	/	1d	1 site	1956-1997, 2007-2014	CHY

remote sensing technology, which can only obtain data after satellite launch, resulting in missing data in early years, the data generated by ERA5-Land have a long time series and can be traced back to 1950. In this study, hourly soil moisture data for the Volumetric soil water layer 1 (0–7 cm) from this dataset are selected.

The daily runoff data at the Tangnaihai hydrometric station are collected from the "China Hydrological Yearbook" (CHY), with data available from 1956–1997 and 2007–2014. The daily precipitation data of 16 rain gauges are provided by the China Meteorological Administration (CMA), ranging from 1960 to 2018.

### 3. Methodology

The framework of the proposed model is shown in Fig. 2. The entire process can be divided into three main parts: (1) Data pre-processing, including data clipping, spatial upscaling, spatiotemporal matching etc.; (2) Establishing a deep neural network model for runoff prediction by combining CNN and LSTM; (3) Model validation and evaluation.

#### 3.1. Data preprocessing

First, all data are standardized to a daily scale. Different time scales can make the neural network training process more difficult and cumbersome. For data with higher temporal resolution, such as Soil Moisture sourced from ERA5-Land dataset, the daily data are obtained by taking the average of the 24-hour data within the same day. For EVI, it can be assumed that its frequency change is slow, then, allow to consider constant in short periods. Therefore, interpolation is used to fill in the missing data in MOD13A1 by replacing with the nearest day in the same month.

Secondly, data sources and platforms have different coverage ranges. Large or irrelevant regions may introduce noise, while small regions may lack information. MOD13A1 data is obtained per tile, with multiple tiles covering the study area. ERA5-Land and GPM\_3IMERGDF data cover the entire globe. To get data for the study area, multiple MOD13A1 tiles taken at the same time are merged. Then, all data (MOD13A1, ERA5-Land, and GPM\_3IMERGDF) is clipped based on the study area's longitude and latitude. ERA5-Land data covers an area from 32.0°N to 36.5°N and 95.55°E to 103.5°E, while GPM\_3IMERGDF and MOD13A1 data cover an area from 31.95°N to 36.45°N and 95.55°E to 103.5°E.

Finally, different data sources have different spatial resolutions. To avoid the large resolution differences that may affect the neural network training performance and reduce the network burden, the spatial resolution of MOD13A1 data is reduced from initial 500 m to 5 km through bilinear interpolation. The spatial resolutions of other data remain unchanged (10 km).

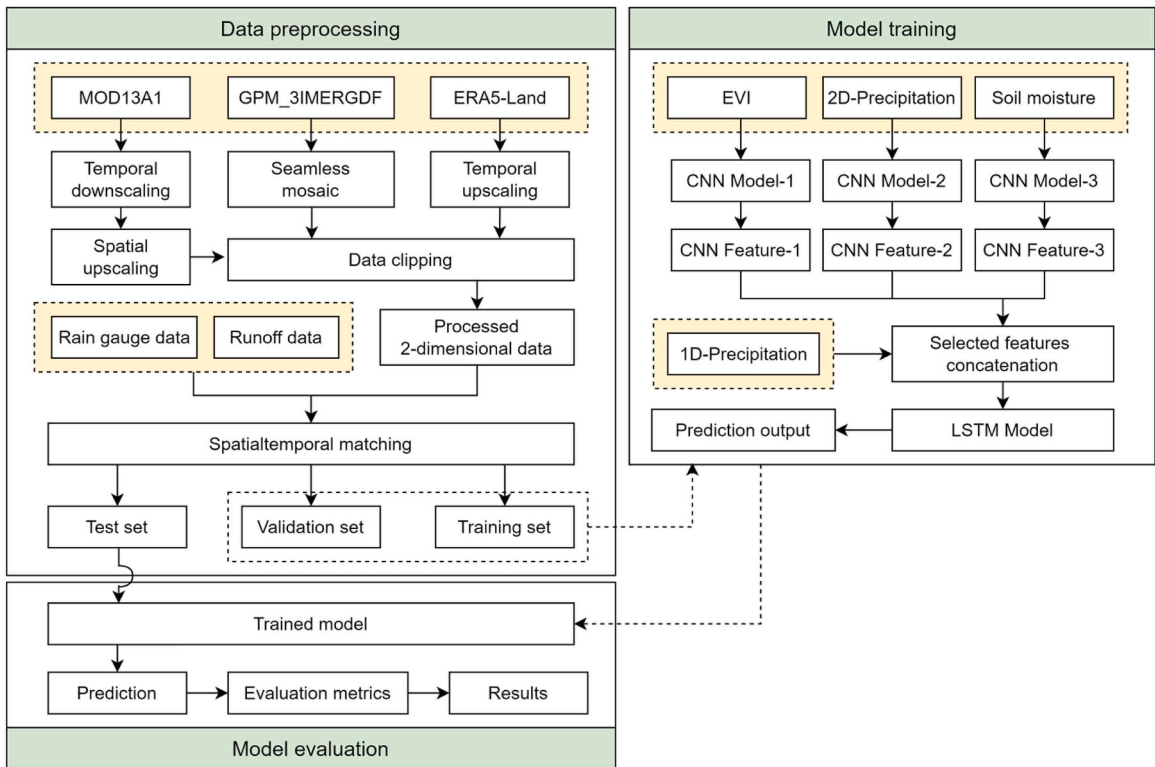


**Fig. 2.** Flow chart of the CNN-LSTM hybrid model. The EVI data is derived from the MOD13A1 product, 2D-Precipitation data is derived from the GPM\_3IMERGDF product, and soil moisture data is derived from the ERA5-Land dataset. Besides, the 1D-Precipitation is sourced from rain gauges.

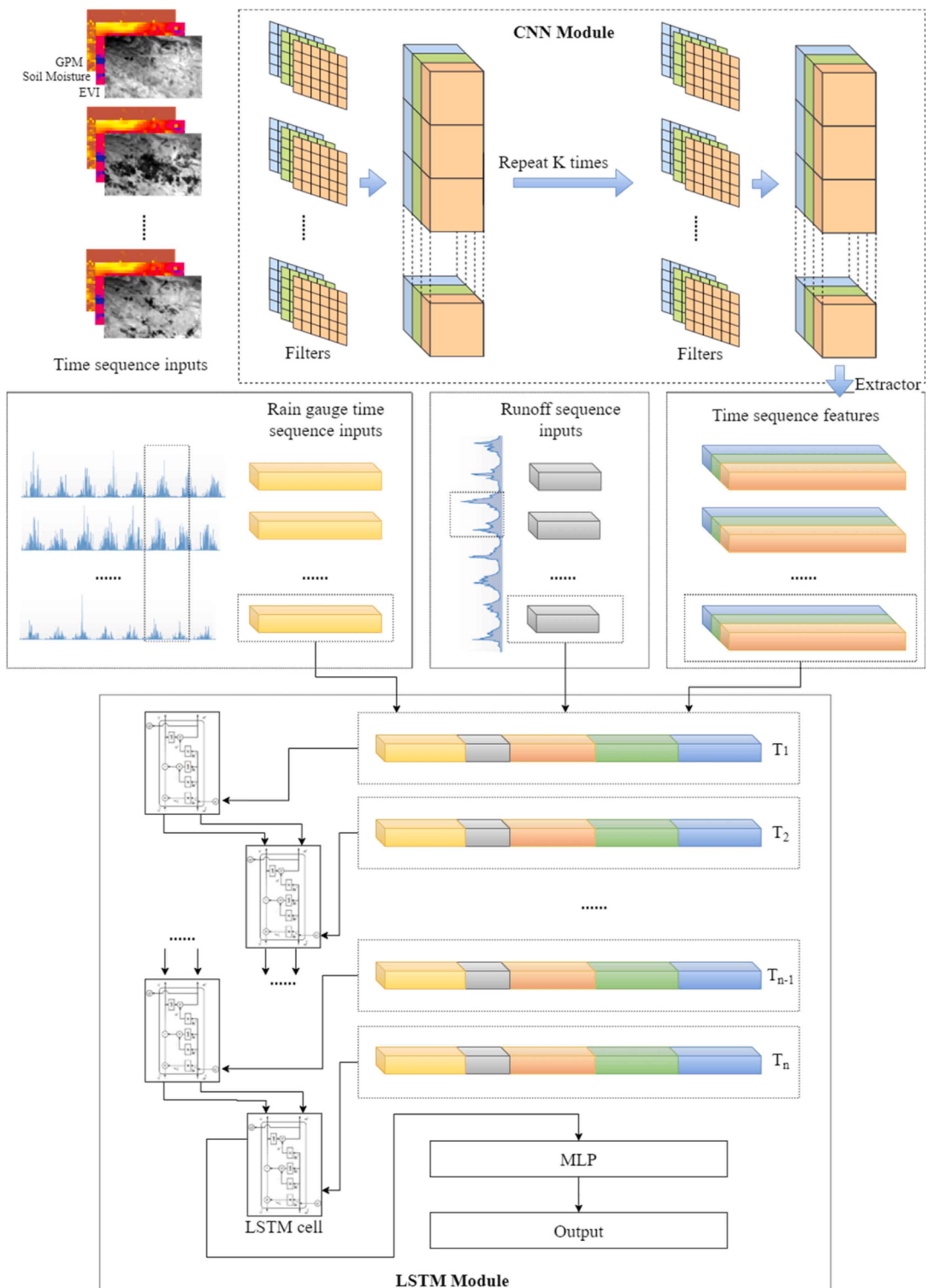


**Fig. 3.** The structure of the CNN-LSTM hybrid model. CNN: convolutional neural networks; LSTM: Long Short-Term Memory Networks; MLP: Multilayer Perceptron.

### 3.2. Basic deep neural network models

Multilayer Perceptron (MLP) is a feedforward neural network composed of multiple neuron layers, usually including input layer, hidden layer, and output layer. It introduces complex feature transformations through nonlinear activation functions, which is one of the foundations of deep learning.

Convolutional neural network (CNN) is widely used in image recognition. It connects neurons between two layers using convolution kernels, which are shared across all images, allowing the images to maintain their original spatial relationships after convolution. The two most distinctive features of CNNs are local perception and weight sharing. Since neurons are connected through the convolution kernel, each neuron is only connected to a subset of neurons in the previous layer and thus perceives locally. Weight sharing refers to the use of the same set of kernel parameters in convolution across the entire image. Local perception and weight sharing greatly reduce the data dimensionality, making CNNs suitable for image processing. The characteristics of CNNs make them naturally advantageous in effectively extracting spatial dependencies of targets and their surroundings.

Long Short-Term Memory (LSTM) is an excellent variant model of Recurrent Neural Networks (RNNs). The structural distinction between LSTM and RNN lies in the inclusion of four gate units: cell state, input gate, forget gate, and output gate. These gate units enable LSTM to retain significant information and filter out irrelevant information. As a result, LSTM is particularly suitable for dealing with problems highly related to time series, especially those with long-term dependencies.

### 3.3. The proposed CNN-LSTM hybrid model

[Fig. 3.](#) illustrates the framework of the proposed CNN-LSTM hybrid model. The hybrid model contains a CNN module for spatial information extraction and an LSTM module for temporal information extraction. The work process of the CNN-LSTM hybrid model is as follows: (1) Multiple independent CNNs are employed to extract spatial information from remote sensing-based and re-analysis datasets. Specifically, for various types of 2D inputs, CNNs adapt their hyperparameters based on input sizes to effectively process different data. During the feature extraction, the whole data is divided into segments using time-windows, with each segment encompassing remote sensing and reanalysis data for all time steps within that interval. These time-windows serve as groundwork for subsequent LSTM learning. Within each time segment, separate CNNs concurrently process respective inputs, extracting information through iterative filtering and aggregation. (2) The CNN-extracted feature vectors, representing underlying surface information, are combined with gauge-based hydro-meteorological features from corresponding time segments and fed into LSTM. Through LSTM learning, relationships among features at different time points are captured, culminating in the acquisition of hidden layer information at the final time step. (3) The features learned by LSTM are input to a Multi-Layer Perceptron (MLP) for further refinement and ultimately generate 1D outcomes.

The detailed structure of the CNN network and specific hyperparameter settings are indicated in [Fig. 4](#). It illustrates the process of

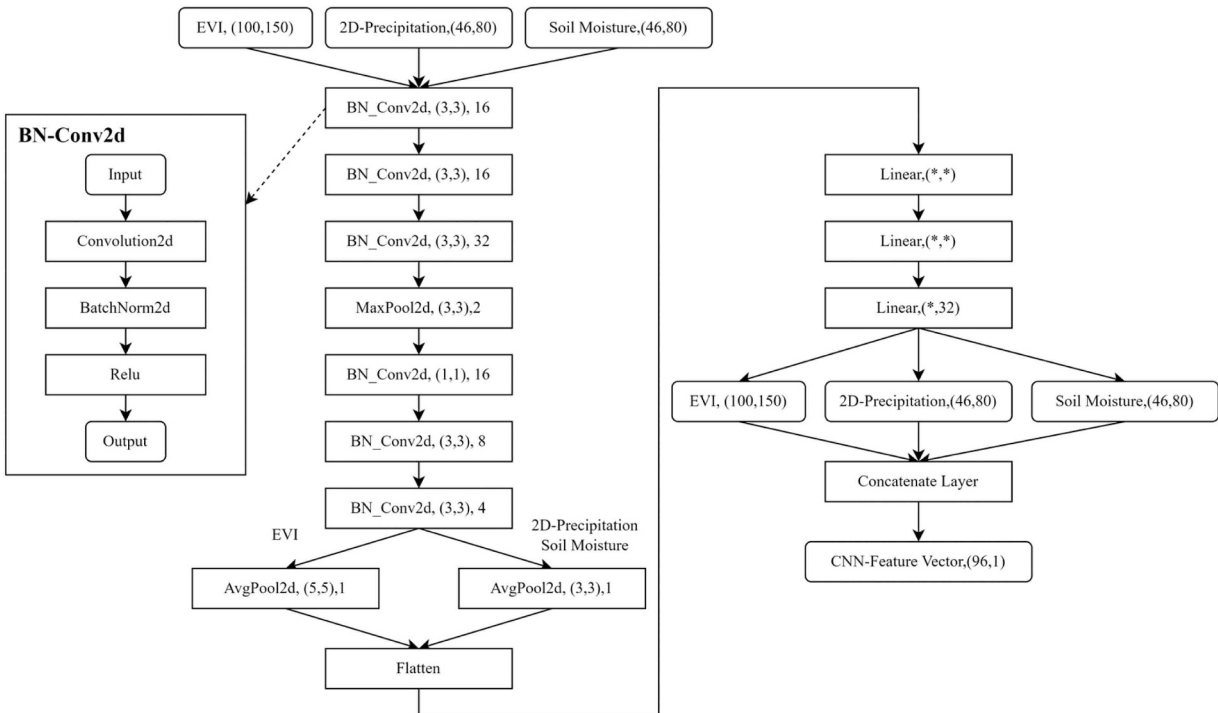


[Fig. 4.](#) The architecture of the CNN.

inputting the underlying surface image at time  $t$  and extracting the feature vector output. According to the size of the input image, CNN selects the network corresponding to the preset hyperparameters to meet the input requirements of different sizes of data. BN\_Conv2d represents a combined network consisting of a traditional 2D convolutional layer (Convolution2d), a 2D normalization layer (BatchNorm2d), and an activation function (ReLU). The hyperparameters of BN\_Conv2d indicate the size and number of convolution kernels. The max pooling layer (MaxPool2d) has translation invariance and can effectively extract texture and contour features and filter out much useless information. The average pooling layer (AvgPool2d) tends to the overall characteristics of the object and can prevent the loss of high-dimensional information. The hyperparameters of the pooling layer respectively represent the size and stride of the convolution kernel. Linear is the fully connected layer that regulates the size of the output vector.

### 3.4. Evaluation metrics

To evaluate the performance of different (environmental) models, please refer to literature published by [Bennett et al. \(2013\)](#). In this study, the Nash–Sutcliffe model Efficiency coefficient (NSE), Mean Absolute Error (MAE), and Root Mean Square Error (RMSE) are selected as evaluation indicators. The indicators are defined by the following equations:

$$\text{RMSE} = \sqrt{\frac{1}{n} \sum_{i=1}^n (y_i - \hat{y}_i)^2} \quad (1)$$

$$\text{MAE} = \frac{1}{n} \sum_{i=1}^n |y_i - \hat{y}_i| \quad (2)$$

$$\text{NSE} = 1 - \frac{\sum_{i=1}^n (y_i - \hat{y}_i)^2}{\sum_{i=1}^n (y_i - \bar{y})^2} \quad (3)$$

Where  $y_i$  and  $\hat{y}_i$  denote the predicted and observed values, respectively.  $\bar{y}$  represents the mean of the predicted values.  $n$  is the number of samples. [Table 2](#) shows an overview of each metric and their typical threshold values.

## 4. Results and discussion

### 4.1. Change characteristics of the in-situ precipitation and runoff

To explore the trend of precipitation and runoff in the study area, a simple linear trend analysis method is used and the results are listed in [Table 3](#).

According to [Table 3](#), combined with the station location information depicted in [Fig. 1](#), it is evident that there is a notable upward trend in precipitation in the southeastern part of the basin (including Jiuzhi, Ruoergai, Banma, and Maqu). This area is predominantly at lower elevations and falls within the Dwc climate zone. Conversely, in the northern and western parts of the basin (including Guinan, Dari, Maduo, Guoluo, and Xinghai), precipitation shows a declining trend, and this region is characterized by relatively higher elevations and falls within the ET climate zone.

Furthermore, the intra-annual distribution of precipitation and runoff depth is examined. [Fig. 5](#) shows the monthly average cumulative precipitation from 2007 to 2014 at different stations. Overall, the rainfall and runoff depth in the basin exhibit similar intra-annual patterns, with a clear seasonal variation. Typically, they peak during the summer months (June and July) and reach their lowest values during the winter months (December, January, and February), indicating a distinct wet-dry seasonality.

In terms of precipitation, the monthly average cumulative values during the dry season usually do not exceed 10 mm. Starting from March, there has been an upward trend, with more significant growth in April and May. By June, the precipitation has significantly increased, reaching its peak in July, with most stations receiving over 100 mm of precipitation. Subsequently, there was a slight decline, followed by a brief rebound in September, and then continued to decline.

It is noteworthy that Songpan experiences its peak precipitation in May, which differs from the other stations. Hongyuan also has relatively high precipitation in May but continues to increase, reaching its peak in July. Maerkang peaks in June. Some stations (Maduo, Xinghai, Guinan, Qumalai) generally receive lower annual precipitation. Considering the information from [Table 3](#) and the [Fig. 5](#), it can be further inferred that the southeastern part of the basin in the Dwc climate zone experiences abundant annual precipitation, which has been increasing over the years, while the northwestern part of the basin in the ET climate zone generally receives less precipitation and exhibits a decreasing trend, except for Shiqu.

**Table 2**

The overview of each metric and their typical threshold values.

Metric	Range	Threshold
RMSE	0 to $\infty$	Context-specific (Lower is better)
MAE	0 to $\infty$	Context-specific (Lower is better)
NSE	- $\infty$ to 1	> 0.75 (Good), 0.36 to 0.75 (Moderate), < 0.36 (Poor)

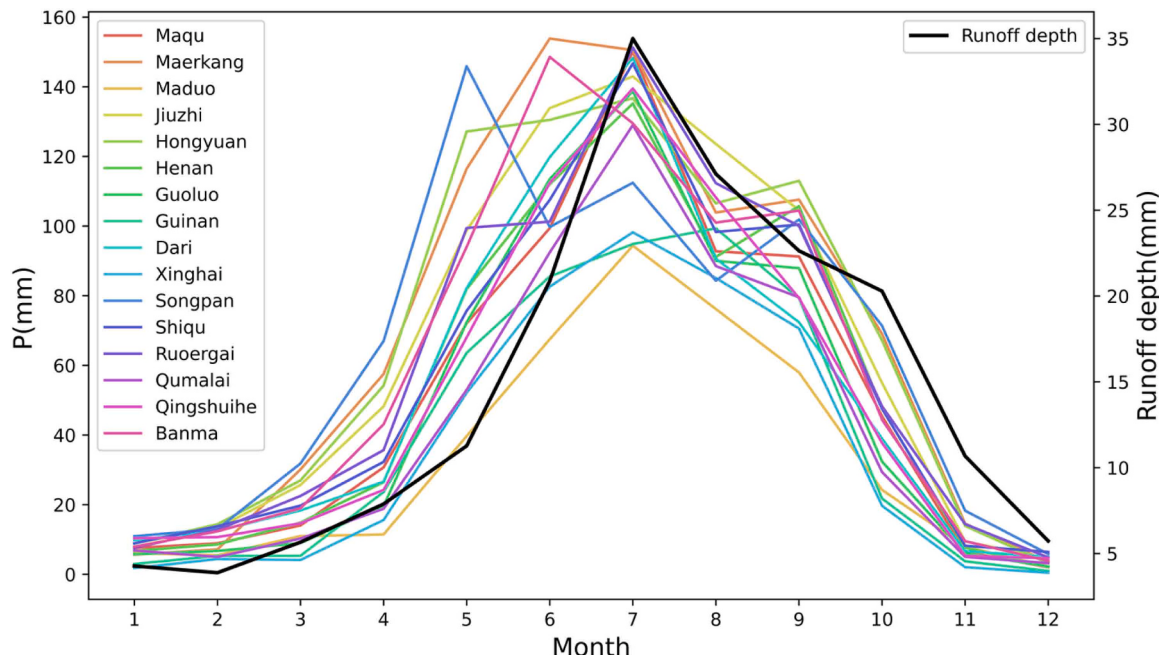
**Table 3**

Linear trend analysis of the in-situ precipitation and runoff.

Site	Maqu	Maerkang	Maduo	Jiuzhi	Hongyuan	Henan	Guoluo	Guinan
Slope	4.871	18.843	-6.549	14.036	34.830*	-27.333*	-14.286	-5.525
Site	Dari	Xinghai	Songpan	Shiqu	Ruoergai	Qumalai	Qingshuihe	Banma
Slope	-6.014	-19.679	17.362	19.196	29.626	-2.467	4.957	12.463

Note:

\* means p-value &lt; 0.05, indicating statistical significance.

**Fig. 5.** Intra-annual distribution of precipitation during 2007–2014 at different rain gauges.

To investigate the precipitation-runoff depth relationship, a linear regression analysis between annual in-situ precipitation and runoff depth is conducted. The results are presented in Table 4. Specifically, the four stations with strong CC between precipitation and runoff depth are Qingshuihe, Maerkang, Maqu, and Maduo. In particular, the slope of Qingshuihe reaches 0.964. It can be approximately assumed that there is a positive correlation between precipitation and runoff depth. Although Maerkang and Maqu have high CC, their slopes are lower. It can be considered that their precipitation and runoff depth are in a certain proportion. Stations with poor correlation include Dari, Ruoergai, Henan, Banma, and Jiuzhi. Relatively, stations in the upper reaches of the basin and surrounding areas have better correlation with runoff depth, while stations with lower correlation are mainly located in the eastern part of the basin (middle and lower reaches). It can be considered that the runoff of SRYRB is closely related to the upstream. However, combined with Fig. 1, it can be clearly observed that the upper reaches of the basin account for almost half of the SRYRB area, with only one station, namely Maduo. Although Qumalai and Qingshuihe are not within the basin, they are geographically close to the upper reaches. These analyzes revealed some limitations of the runoff prediction in SRYRB, namely the lack of gauged data in upstream areas that have important impacts on runoff within the basin. This paves the way for further research exploring image data as solutions for runoff prediction.

**Table 4**

Correlation analysis between precipitation and runoff at individual rain gauges.

Site	Maqu	Maerkang	Maduo	Jiuzhi	Hongyuan	Henan	Guoluo	Guinan
Runoff coefficient	0.400*	0.228*	0.381*	0.121	0.181	0.046	0.289	0.303
CC	0.825	0.850	0.752	0.293	0.660	0.137	0.529	0.636
Site	Dari	Xinghai	Songpan	Shiqu	Ruoergai	Qumalai	Qingshuihe	Banma
Runoff coefficient	0.107	0.139	0.189	0.135	0.035	0.527	0.964 *	0.109
CC	0.121	0.307	0.567	0.498	0.130	0.694	0.963	0.239

Note: CC, Pearson correlation coefficient.

\* p-value &lt; 0.05, indicating statistical significance.

#### 4.2. Runoff prediction results

The data series (2007–2014) are divided into a training set, a validation set and a testing set with a ratio of 7:2:1. Select the best-performing trained model through the validation set to ensure the generalization ability of the model. In order to showcase the effectiveness of the proposed CNN-LSTM model, the study compares it with the standalone LSTM and CNN model. The standalone LSTM model only utilizes the gauge-based hydro-meteorological data (i.e., precipitation) as inputs, while standalone CNN model and the hybrid model supplements image based meteorological data (i.e., precipitation) and underlying surface data (i.e., EVI and soil moisture). For convenience, P is used to denote gauged precipitation in last day ( $P_t$ ); Similarly, GPM denotes 2D-precipitation and SM denotes the Soil moisture. \* means the variable used in the model. Results are shown in [Table 5](#).

For the standalone LSTM model, solely using rain gauge data as input is not enough to predict runoff well (Shown in [Fig. 6](#)). Although the model can fit the overall trend to some extent, it is insufficient in capturing peaks. What is more obvious is that the performance of the LSTM model drops significantly when generalizing to new data, which can be seen from the NSE on the validation set falling from 0.890 to less than 0.6 on the test set. This may imply that during the test period, the watershed's runoff patterns experienced new changes that are not captured by some rain gauges. For standalone CNN, both station precipitation and remote sensing precipitation have certain predictive effects. Although CNN performs worse than LSTM in the validation set, the opposite results are observed in the test set. This reflects that CNN has good generalization performance.

For CNN-LSTM model, it should be noted that the experiment with the input ( $P + \text{EVI}$ ) are considered invalid due to the relatively unqualified NSE (<0.36, poor). On the validation set, the combination of ( $P + \text{GPM} + \text{SM}$ ) provides the best prediction results, as shown in [Fig. 7](#). It also has the highest NSE (0.834) on the test set, indicating that the model under this combination can generalize well to unseen data. GPM data is also critical to the performance of the model, and its absence results in a significant decrease in NSE on the test set. Although EVI as a separate feature cannot support prediction, its addition has a positive impact on improving the performance on the validation set. But EVI does not effectively help on the test set. SM can effectively support  $P$  to improve prediction performance, especially when GPM also exists.

Ground station precipitation are generally considered to be more accurate and can provide strong information for models. GPM and EVI provide large-scale remote sensing data, which fill possible gaps in ground station data in space. Soil moisture is critical to runoff because it determines how much precipitation is absorbed by the soil, which in turn affects runoff. In summary, the combined effect of underlying surface and meteorological conditions affects the generation, movement, and final distribution of runoff. Various experimental results show that the CNN-LSTM model structure can capture spatial features (via CNN) and time series dependencies (via LSTM), and the combination of different data inputs may affect the learning effect of the model in different ways. It also shows that effective selection and fusion of multi-source data is beneficial to improving the prediction ability and generalization ability of the model.

#### 4.3. Model feasibility analysis in the ungauged basin

Although the CNN-LSTM model improved the accuracy of runoff prediction, it still used rain gauge data as one of the inputs, which makes the model rely on gauge-based observations. In fact, many basins worldwide are ungauged or insufficiently gauged. Although remote sensing data may not be as accurate as gauged data, its broad and continuous spatial distribution characteristics make it a potentially effective substitute for areas without ground stations. Therefore, this section aims to verify, based on the above studies, whether remote sensing data or re-analysis data, especially rainfall data provided by the GPM, can be used as an effective substitute for gauged precipitation data to conduct rainfall-runoff analysis. The experiment results are presented in [Table 6](#).

Under different input combinations, the performance of the CNN-LSTM model on the validation set and test set is different. Among them, three sets of experiments with input respectively (EVI), (EVI+SM), and (SM) are considered invalid due to relatively unqualified NSE (<0.0). This shows that it is not feasible to use EVI or SM alone or a combination of the two to predict runoff in the basin. However, the prediction effect is significant when using only GPM both on the validation set (0.849) and the test set (0.720). GPM data has a greater contribution to the generalization ability of the model. It is proved that GPM within the basin has certain substitutability for

**Table 5**

Runoff prediction results of different models.

Model	Input data				Validation period			Test period		
	P	GPM	EVI	SM	RMSE	MAE	NSE	RMSE	MAE	NSE
LSTM	*				171.214	131.972	0.890	320.808	233.009	0.510
CNN	*				196.670	142.159	0.854	285.184	228.591	0.612
	*				208.928	136.459	0.836	290.047	225.166	0.599
CNN-LSTM	*	*			242.545	153.921	0.779	238.215	169.272	0.730
	*	*	*		204.979	138.939	0.842	248.093	177.753	0.707
	*	*		*	166.706	111.809	0.895	186.512	142.460	0.834
	*		*		\	\	\	\	\	\
	*			*	240.411	169.596	0.783	307.910	184.455	0.549
	*		*	*	222.658	135.822	0.813	310.156	219.541	0.542
	*	*	*	*	221.388	154.376	0.816	218.724	130.491	0.772

Note: \, null value, indicating invalid result.

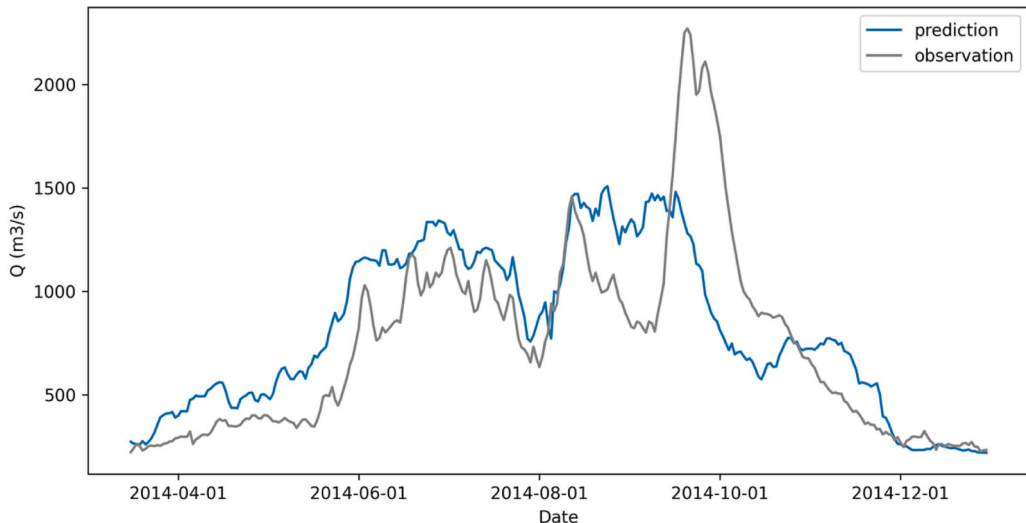


**Fig. 6.** Runoff prediction using LSTM (NSE=0.510) compared with the observed runoff.

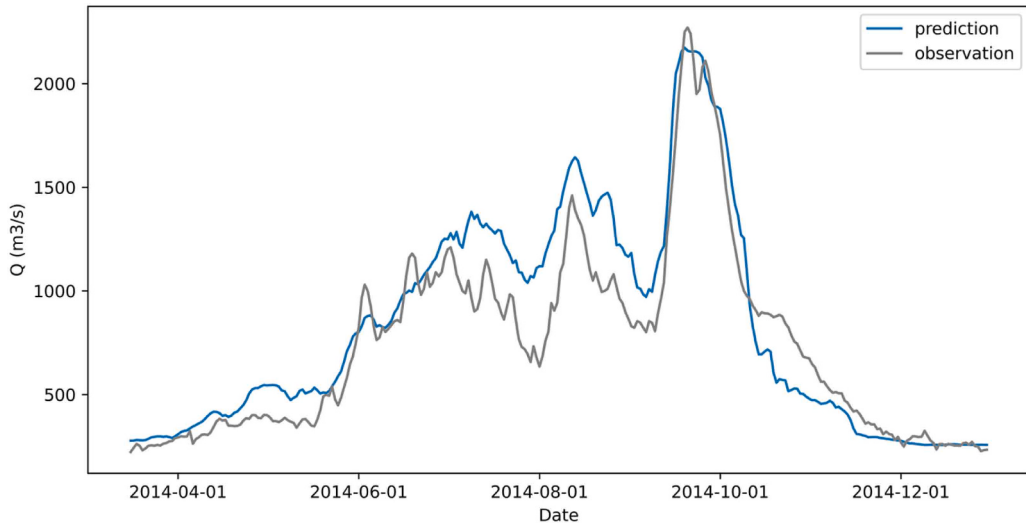


**Fig. 7.** Runoff prediction driven by P, GPM, and SM using CNN-LSTM Model (NSE=0.834) compared with the observed runoff.

**Table 6**

Runoff prediction results of the CNN-LSTM model without using in-situ data.

Input	Validation			Test					
	GPM	EVI	SM	RMSE	MAE	NSE	RMSE	MAE	NSE
*				200.535	142.981	0.849	242.310	179.384	0.720
*	*			184.232	136.200	0.872	269.300	192.150	0.655
*		*		157.670	111.483	0.906	190.882	141.999	0.827
*		*	*	\	\	\	\	\	\
*		*	*	\	\	\	\	\	\
*	*	*	*	157.549	112.583	0.907	253.272	180.006	0.695

Note: \, null value, indicating invalid result.

site runoff. Compared with ground stations, GPM provides more general precipitation information. It is worth noting that although SM alone is ineffective, it has a certain auxiliary effect on GPM. (GPM+SM) is currently the second-best input except (P + GPM+SM). The test set NSE reaches 0.827, which is close to and second only to the use of in-situ data. This result just illustrates the complexity of

runoff, which is affected by multiple factors such as underlying surface and climate, and a single meteorological factor cannot fully characterize it. The situation of EVI is opposite to that of SM. The combination of (GPM+EVI) has excellent effect on the verification set, but drops significantly to 0.655 on the test set. On the one hand, the reason is that the time resolution of EVI is too low, and simple repetitive filling makes overfitting prone to occur in the model training phase. On the other hand, the possible reason is that the characteristics of the test set data have changed. From a physical perspective, the CNN-LSTM model cannot capture the immediate response of runoff to actual vegetation conditions, resulting in time lag and the inability to quickly adapt to changes on the test set. Despite this, the combined input in the validation set (GPM+EVI) has very excellent results, which to a certain extent illustrates the contribution and impact of EVI on runoff changes. (GPM+EVI+SM) is the same. In short, the study provides a promising tool for runoff prediction in ungauged or insufficiently basins.

In order to further verify the hypothesis that "the characteristics of the test set data have changed" proposed in the above analysis, the study divides all data into three time periods according to the training set, validation set and test set, and performs monthly linear analysis on the measured precipitation and observed runoff respectively. Fig. 8 shows the results of CC between them. Fig. 9.

There are significant differences in the monthly scale CC of precipitation and runoff depth among the test set, training set, and validation set. In most stations, the CC of the training set and validation set are higher than those of the test set, and exhibit a relatively consistent correlation between rainfall and runoff depth. On the test set, different stations show significant differences, especially Maerkang (as shown in the figure). It can be considered that the relationship between rainfall and runoff within the watershed has undergone certain changes during the validation and test sets. This provides a certain degree of interpretability for the significant decrease in test set performance of the model under certain input combinations. Nevertheless, GPM still performs relatively well as input on the test set in most cases, further demonstrating its support for the generalization ability of CNN-LSTM models. It also can be considered that the model still has good performance even when the external changes are relatively small.

#### 4.4. Discussion

This study explores the feasibility of the CNN-LSTM model in runoff prediction in SRYRB, and focuses on the fusion of multi-source data and the applicability of the model in data-scarce areas.

##### 4.4.1. Model performance and multi-source data

The complex underlying surface characteristics and changing climate conditions of SRYRB require hydrological models to be highly adaptable and accurate. Single station data cannot reflect spatial heterogeneity under complex terrain conditions. As one of the core modules of CNN-LSTM, the CNNs can effectively fuse and analyze image data from different sources, which not only enhances the model's ability to capture internal spatial patterns in the basin, but also effectively enhances generalization.

##### 4.4.2. Spatial characteristics of image data

The addition of image data significantly improves the model's spatial analysis capabilities in SRYRB. Specifically, the long-term comprehensive coverage of GPM precipitation data provides the model with extensive and continuous precipitation information, which is critical to ensuring consistent model performance across the entire basin. In addition, although the EVI and SM data alone are not sufficient for effective runoff prediction, they provide the model with detailed information about region-specific hydrological conditions. The introduction of these data enables the model to gain a deeper understanding of the complex spatial relationship between precipitation and runoff, thereby improving the accuracy of runoff predictions based on precipitation data.

##### 4.4.3. Feasibility of application in areas lacking data

In the study area, especially the upstream areas that have a greater impact on runoff, ground stations are scarce, which restricts the application and accuracy of traditional hydrological models. In this case, available image data such as remote sensing data is a key resource for obtaining information on surface characteristics. It provides wider geographical coverage and temporal continuity. Experimental results prove that through the CNN-LSTM model, these remote sensing data can be successfully used to supplement or replace in-situ data, with high model accuracy and reliability. This makes runoff prediction feasible in data-scarce areas.

Although this study has achieved certain results in applying the CNN-LSTM model to runoff prediction in SRYRB, it also has some limitations. First, the EVI data used have limited temporal resolution, which limits the model's ability to utilize information on the underlying surface vegetation. Secondly, only three factors, namely precipitation, soil moisture and vegetation index, are considered in the study, which may not be enough to fully reflect the evolution trend of runoff. Finally, during the testing process, it has been found that although the model shows certain generalization ability and robustness, the performance of the model degraded when face with significant changes in data distribution.

To overcome these limitations, future research will explore the following aspects: First, obtain vegetation index data with higher temporal resolution to capture changes more accurately in underlying surface vegetation. Second, a wider variety of underlying surfaces and meteorological factors will be considered to describe and predict runoff processes more fully. Finally, explore how to improve the model's generalization ability in changing environments. This might include developing more advanced machine learning algorithms, or leveraging more diverse training data sets to enhance the model's adaptability to new situations. These improvements are expected to lead to more accurate and robust results in future hydrological prediction efforts.

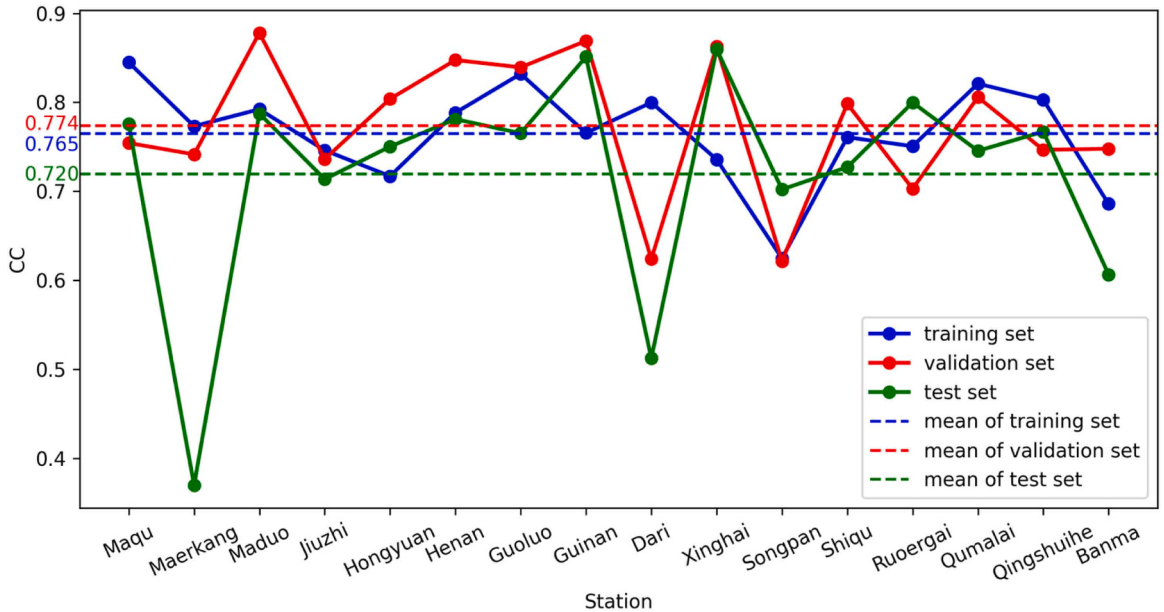


**Fig. 8.** CC of precipitation and runoff depth at different stations in different periods.

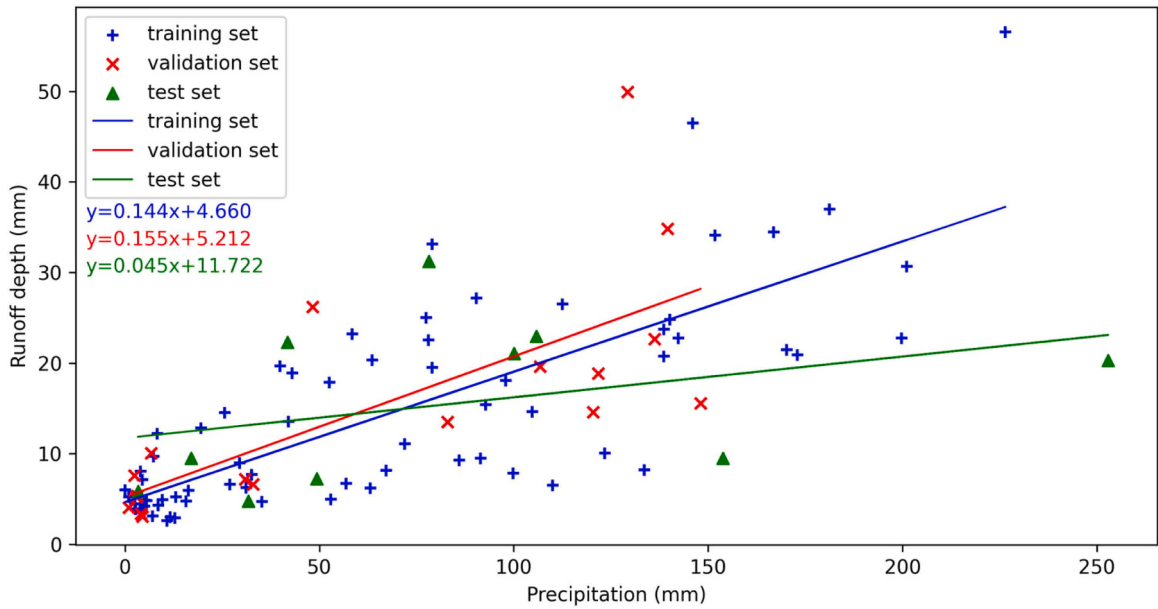


**Fig. 9.** CC between precipitation and runoff depth at the Maerkang station over different (training, validation, test) periods.

## 5. Conclusion

Incorporating multiple grid-based data such as GPM, EVI and SM into the CNN-LSTM hybrid model, this study aims to improve daily runoff prediction accuracy in the Source Region of the Yellow River basin. The hybrid model driven by the in-situ precipitation, GPM, and SM data achieved the best result with NSE of 0.834, outperforming the single models (LSTM, CNN). It also reached a comparable result (NSE=0.827) even with the driven data with only GPM and SM data. Results imply that grid based data can represent the spatiotemporal variations of the precipitation and underlying surface of the study basin and the hybrid model has good ability on capturing their spatiotemporal variation features. However, the model degrades when rainfall-runoff relationship changes. Future research needs to introduce more high-quality data sets and explore new model architectures to cope with changing environment.

## CRediT authorship contribution statement

**Shao Junming:** Writing – review & editing, Funding acquisition, Conceptualization. **Luo Zhengming:** Writing – review & editing. **Wang Guoqing:** Writing – review & editing, Funding acquisition. **Hu Feichi:** Writing – original draft, Formal analysis. **Yang Junran:** Writing – review & editing. **Yang Qinli:** Writing – review & editing, Writing – original draft, Supervision, Funding acquisition, Conceptualization.

## Declaration of Competing Interest

The authors declare that they have no known competing financial interests or personal relationships that could have appeared to influence the work reported in this paper.

## Data Availability

Data will be made available on request.

## Acknowledgments

This work has been financially supported by the National Key Research and Development Program of China [grant number 2021YFC3201100], the National Natural Science Foundation of China [grant numbers 52079026 and 61976044], Sichuan Science and Technology Program [grant number 2022YFG0260], Chengdu Science and Technology Program [grant number 2021-YF08-00127-GX], Municipal Government of Quzhou [2023D016], and the Fundamental Research Funds for the Central Universities [grant number ZYGX2019Z014].

## References

- Abrahart, R.J., See, L., 2000. Comparing neural network and autoregressive moving average techniques for the provision of continuous river flow forecasts in two contrasting catchments. *Hydrol. Process.* 14 (11–12), 2157–2172. [https://doi.org/10.1002/1099-1085\(20000815/30\)14:11/12<2157::AID-HYP57>3.0.CO;2-S](https://doi.org/10.1002/1099-1085(20000815/30)14:11/12<2157::AID-HYP57>3.0.CO;2-S).
- Balsamo, G., Albergel, C., Beljaars, A., Boussetta, S., Brun, E., Cloke, H., Vitart, F., 2015. ERA-Interim/Land: a global land surface reanalysis data set. *Hydrol. Earth Syst. Sci.* 19 (1), 389–407.
- Bengtsson, L., Hagemann, S., Hodges, K.I., 2004. Can climate trends be calculated from reanalysis data? *J. Geophys. Res.: Atmos.* 109 (D11).
- Bennett, N.D., Croke, B.F.W., Guariso, G., Guillaume, J.H.A., Hamilton, S.H., Jakeman, A.J., Marsili-Libelli, S., Newham, L.T.H., Norton, J.P., Perrin, C., Pierce, S.A., Robson, B., Seppelt, R., Voinov, A.A., Fath, B.D., Andreassian, V., 2013. Characterising performance of environmental models. *Environ. Model. Softw.* 40, 1–20. <https://doi.org/10.1016/j.envsoft.2012.09.011>.
- Breiman, L., 2001. Random forests. *Mach. Learn.* 45 (1), 5–32. <https://doi.org/10.1023/A:1010933404324>.
- Chen, T., Guestrin, C., 2016. XGBoost: a scalable tree boosting system. *Proc. 22nd ACM SIGKDD Int. Conf. Knowl. Discov. Data Min.* 785–794. <https://doi.org/10.1145/2939672.2939785>.
- Dibike, Y.B., Velickov, S., Solomatine, D., Abbott, M.B., 2001. Model induction with support vector machines: introduction and applications. *J. Comput. Civ. Eng.* 15 (3), 208–216. [https://doi.org/10.1061/\(ASCE\)0887-3801\(2001\)15:3\(208\)](https://doi.org/10.1061/(ASCE)0887-3801(2001)15:3(208)).
- Gassman, P.W., Sadeghi, A.M., Srinivasan, R., 2014. Applications of the SWAT model special section: overview and insights. *J. Environ. Qual.* 43 (1), 1–8. <https://doi.org/10.2134/jeq2013.11.0466>.
- Guan, X., Zhang, J., Elmahdi, A., Li, X., Liu, J., Liu, Y., Jin, J., Liu, Y., Bao, Z., Liu, C., He, R., Wang, G., 2019. The capacity of the hydrological modeling for water resource assessment under the changing environment in Semi-Arid River Basins in China. *Article 7 Water* 11 (7). <https://doi.org/10.3390/w11071328>.
- Guo, B., Wei, C., Yu, Y., Liu, Y., Li, J., Meng, C., Cai, Y., 2022. The dominant influencing factors of desertification changes in the source region of Yellow River: climate change or human activity? *Sci. Total Environ.* 813, 152512 <https://doi.org/10.1016/j.scitotenv.2021.152512>.
- Ibrahim, K.S.M.H., Huang, Y.F., Ahmed, A.N., Koo, C.H., El-Shafie, A., 2022. A review of the hybrid artificial intelligence and optimization modelling of hydrological streamflow forecasting. *Alex. Eng. J.* 61 (1), 279–303. <https://doi.org/10.1016/j.aej.2021.04.100>.
- Islam, K.I., Elias, E., Carroll, K.C., Brown, C., 2023. Exploring random forest machine learning and remote sensing data for streamflow prediction: an alternative approach to a process-based hydrologic modeling in a snowmelt-driven watershed. *Article 16 Remote Sens.* 15 (16). <https://doi.org/10.3390/rs15163999>.
- Jin, S., Zheng, Z., Ning, L., 2021. Separating variance in the runoff in Beijing's river system under climate change and human activities. *Phys. Chem. Earth, Parts A/B/C* 123, 103044.
- Kwon, M., Kwon, H.-H., Han, D., 2020. A hybrid approach combining conceptual hydrological models, support vector machines and remote sensing data for rainfall-runoff modeling. *Article 11 Remote Sens.* 12 (11). <https://doi.org/10.3390/rs12111801>.
- Lee, Y.H., Singh, V.P., 2005. Tank model for sediment yield. *Water Resour. Manag.* 19 (4), 349–362. <https://doi.org/10.1007/s11269-005-7998-y>.
- Li, P., Zhang, J., Krebs, P., 2022. Prediction of flow based on a CNN-LSTM combined deep learning approach. *Article 6 Water* 14 (6). <https://doi.org/10.3390/w14060993>.
- Li, Q., Yang, M., Wan, G., Wang, X., 2016. Spatial and temporal precipitation variability in the source region of the Yellow River. *Environ. Earth Sci.* 75, 1–14.
- Li, W., Kiaghadi, A., Dawson, C., 2021. High temporal resolution rainfall-runoff modeling using long-short-term-memory (LSTM) networks. *Neural Comput. Appl.* 33, 1261–1278.
- Liu, H., Yang, Q., Liu, Z., Shao, J., Wang, G., 2023. An attention-mechanism-based deep fusion model for improving quantitative precipitation estimation in a sparsely-gauged basin. *J. Hydrol.*, 130568.
- Luan, Y., Lin, S., 2019. Research on text classification based on CNN and LSTM (March). *2019 IEEE International Conference on Artificial Intelligence and Computer Applications (ICAICA)*. IEEE, pp. 352–355 (March).
- Lv, Z., Zuo, J., Rodriguez, D., 2020. Predicting of runoff using an optimized SWAT-ANN: a case study. *J. Hydrol.: Reg. Stud.* 29, 100688.
- Ma, L., He, C., Bian, H., Sheng, L., 2016. MIKE SHE modeling of ecohydrological processes: Merits, applications, and challenges. *Ecol. Eng.* 96, 137–149. <https://doi.org/10.1016/j.ecoleng.2016.01.008>.
- Man, Y., Yang, Q., Shao, J., Wang, G., Bai, L., Xue, Y., 2023. Enhanced LSTM model for daily runoff prediction in the Upper Huai River Basin, China. *Engineering* 24, 229–238. <https://doi.org/10.1016/j.eng.2021.12.022>.
- Meng, F., Su, F., Yang, D., Tong, K., Hao, Z., 2016. Impacts of recent climate change on the hydrology in the source region of the Yellow River basin. *J. Hydrol.: Reg. Stud.* 6, 66–81. <https://doi.org/10.1016/j.ejrh.2016.03.003>.

- Mishra, P.K., Karmakar, S., Guhathakurta, P., 2016. A broad literature survey of development and application of artificial neural networks in rainfall-runoff modelling. In: Pant, M., Deep, K., Bansal, J.C., Nagar, A., Das, K.N. (Eds.), Proceedings of Fifth International Conference on Soft Computing for Problem Solving. Springer, pp. 691–710. [https://doi.org/10.1007/978-981-10-0451-3\\_62](https://doi.org/10.1007/978-981-10-0451-3_62).
- Moukomla, S., Blanken, P.D., 2017. The estimation of the North American Great Lakes turbulent fluxes using satellite remote sensing and MERRA reanalysis data. *Remote Sens.* 9 (2), 141.
- Pradhan, R.K., Markonis, Y., Vargas Godoy, M.R., Villalba-Pradas, A., Andreadis, K.M., Nikolopoulos, E.I., Papalexiou, S.M., Rahim, A., Tapiador, F.J., Hanel, M., 2022. Review of GPM IMERG performance: a global perspective. *Remote Sens. Environ.* 268, 112754 <https://doi.org/10.1016/j.rse.2021.112754>.
- Ren, Y., Liu, J., Shalamzari, M.J., Arshad, A., Liu, S., Liu, T., Tao, H., 2022. Monitoring recent changes in drought and wetness in the source region of the Yellow River Basin, China. *Article 6 Water* 14 (6). <https://doi.org/10.3390/w14060861>.
- Riad, S., Mania, J., Bouchaou, L., Najjar, Y., 2004. Rainfall-runoff model using an artificial neural network approach. *Math. Comput. Model.* 40 (7), 839–846. <https://doi.org/10.1016/j.mcm.2004.10.012>.
- Shen, Q., Cong, Z., Lei, H., 2017. Evaluating the impact of climate and underlying surface change on runoff within the Budyko framework: A study across 224 catchments in China. *J. Hydrol.* 554, 251–262.
- Shi, P., Chen, C., Srinivasan, R., Zhang, X., Cai, T., Fang, X., Qu, S., Chen, X., Li, Q., 2011. Evaluating the SWAT Model for Hydrological Modeling in the Xixian Watershed and a Comparison with the XAJ Model. *Water Resour. Manag.* 25 (10), 2595–2612. <https://doi.org/10.1007/s11269-011-9828-8>.
- Sit, M., Demiray, B.Z., Xiang, Z., Ewing, G.J., Sermet, Y., Demir, I., 2020. A comprehensive review of deep learning applications in hydrology and water resources. *Water Sci. Technol.* 82 (12), 2635–2670. <https://doi.org/10.2166/wst.2020.369>.
- Smith, E.A., Asrar, G., Furuhama, Y., Ginati, A., Mugnai, A., Nakamura, K., Adler, R.F., Chou, M.-D., Desbois, M., Durning, J.F., Entin, J.K., Einaudi, F., Ferraro, R.R., Guzzi, R., Houser, P.R., Hwang, P.H., Iguchi, T., Joe, P., Kakar, R., Zhang, W., 2007. International global precipitation measurement (GPM) program and mission: an overview. In: Levizzani, V., Bauer, P., Turk, F.J. (Eds.), *Measuring Precipitation From Space: EURAINSAT and the Future*. Springer Netherlands, pp. 611–653. [https://doi.org/10.1007/978-1-4020-5835-6\\_48](https://doi.org/10.1007/978-1-4020-5835-6_48).
- Song, X., Yang, G., Yan, C., Duan, H., Liu, G., Zhu, Y., 2009. Driving forces behind land use and cover change in the Qinghai-Tibetan Plateau: A case study of the source region of the Yellow River, Qinghai Province, China. *Environ. Earth Sci.* 59 (4), 793–801. <https://doi.org/10.1007/s12665-009-0075-8>.
- Staudemeyer, R.C., & Morris, E.R. (2019). *Understanding LSTM – a tutorial into Long Short-Term Memory Recurrent Neural Networks* (arXiv:1909.09586). arXiv. (<https://doi.org/10.48550/arXiv.1909.09586>).
- Tang, G., Clark, M.P., Papalexiou, S.M., Ma, Z., Hong, Y., 2020. Have satellite precipitation products improved over last two decades? A comprehensive comparison of GPM IMERG with nine satellite and reanalysis datasets. *Remote Sens. Environ.* 240, 111697 <https://doi.org/10.1016/j.rse.2020.111697>.
- Tokar, A.S., Johnson, P.A., 1999. Rainfall-runoff modeling using artificial neural networks. *J. Hydrol. Eng.* 4 (3), 232–239. [https://doi.org/10.1061/\(ASCE\)1084-0699\(1999\)4:3\(232\)](https://doi.org/10.1061/(ASCE)1084-0699(1999)4:3(232)).
- Xiang, Z., Yan, J., Demir, I., 2020. A rainfall-runoff model with LSTM-based sequence-to-sequence learning. *Water Resour. Res.* 56 (1), e2019WR025326 <https://doi.org/10.1029/2019WR025326>.
- Xin, J., Sun, X., Liu, L., Li, H., Liu, X., Li, X., Xu, Z., 2021. Quantifying the contribution of climate and underlying surface changes to alpine runoff alterations associated with glacier melting. *Hydrol. Process.* 35 (3), e14069.
- Xu, T., Liang, F., 2021. Machine learning for hydrologic sciences: an introductory overview. *WIREs Water* 8 (5), e1533. <https://doi.org/10.1002/wat2.1533>.
- Xu, Y., Liu, Y., Jiang, Z., Yang, X., Wang, X., Zhang, Y., Qin, Y., 2022. Improved convolutional neural network and its application in non-periodical runoff prediction. *Water Resour. Manag.* 36 (15), 6149–6168. <https://doi.org/10.1007/s11269-022-03346-3>.
- Yan, R., Liao, J., Yang, J., Sun, W., Nong, M., Li, F., 2021. Multi-hour and multi-site air quality index forecasting in Beijing using CNN, LSTM, CNN-LSTM, and spatiotemporal clustering. *Expert Syst. Appl.* 169, 114513.
- Yang, M., Yang, Q., Shao, J., Wang, G., Zhang, W., 2023. A new few-shot learning model for runoff prediction: demonstration in two data scarce regions. *Environ. Model. Softw.* 162, 105659 <https://doi.org/10.1016/j.envsoft.2023.105659>.
- Yang, Q., Zhang, H., Wang, G., Luo, S., Chen, D., Peng, W., Shao, J., 2019. Dynamic runoff simulation in a changing environment: a data stream approach. *Environ. Model. Softw.* 112, 157–165.
- Yin, H., Zhang, X., Wang, F., Zhang, Y., Xia, R., Jin, J., 2021. Rainfall-runoff modeling using LSTM-based multi-state-vector sequence-to-sequence model. *J. Hydrol.* 598, 126378.
- Yuan, F., Berndtsson, R., Zhang, L., Uvo, C.B., Hao, Z., Wang, X., Yasuda, H., 2015. Hydro climatic trend and periodicity for the source region of the Yellow River. *J. Hydrol. Eng.* 20 (10), 05015003 [https://doi.org/10.1061/\(ASCE\)HE.1943-5584.0001182](https://doi.org/10.1061/(ASCE)HE.1943-5584.0001182).
- Yuan, X., Chen, C., Lei, X., Yuan, Y., Muhammad Adnan, R., 2018. Monthly runoff forecasting based on LSTM-ALO model. *Stoch. Environ. Res. Risk Assess.* 32 (8), 2199–2212. <https://doi.org/10.1007/s00477-018-1560-y>.
- Zhou, F., Chen, Y., Liu, J., 2023. Application of a new hybrid deep learning model that considers temporal and feature dependencies in rainfall-runoff simulation. *Remote Sens.*, 15(5), Artic. 5. <https://doi.org/10.3390/rs15051395>.
- Zhou, W., Peng, B., Shi, J., Wang, T., Dhital, Y.P., Yao, R., Zhao, R., 2017. Estimating high resolution daily air temperature based on remote sensing products and climate reanalysis datasets over glacierized basins: a case study in the Langtang Valley, Nepal. *Remote Sens.* 9 (9), 959.
- Zhou, W., Zhu, Z., Xie, Y., Cai, Y., 2021. Impacts of rainfall spatial and temporal variabilities on runoff quality and quantity at the watershed scale. *J. Hydrol.* 603, 127057.